

# Experimental estimation of deviation frequency within the spectrum of scintillations of the carrier phase of GNSS signals

Vladislav Demyanov <sup>1,2,\*</sup>, Ekaterina Danilchuk <sup>3</sup>, Yury Yasyukevich <sup>1,3</sup> and Maria Sergeeva <sup>4,5</sup>

<sup>1</sup> Institute of Solar Terrestrial Physics, Siberian Branch Russian Academy of Sciences, Irkutsk 664033, Russia; [vv.emyanov@gmail.com](mailto:vv.emyanov@gmail.com)

<sup>2</sup> Irkutsk State Transport University, Irkutsk 664074, Russia; [demyanov\\_vv@irgups.ru](mailto:demyanov_vv@irgups.ru)

<sup>3</sup> Irkutsk State University, Irkutsk, Russia 664003; [danilchuk.k@mail.ru](mailto:danilchuk.k@mail.ru)

<sup>4</sup> 4SCiESMEX, LANCE, Instituto de Geofísica, Unidad Michoacán, Universidad Nacional Autónoma de México, Antigua Carretera a Patzcuaro 8701, Morelia, Michoacán, C.P.58089, México; [maria.a.sergeeva@gmail.com](mailto:maria.a.sergeeva@gmail.com)

<sup>5</sup> 5CONACYT, Instituto de Geofísica, Unidad Michoacán, Universidad Nacional Autónoma de México, Antigua Carretera a Patzcuaro 8701, Morelia, Michoacán, C.P.58089, México

\* Correspondence: [vv.emyanov@gmail.com](mailto:vv.emyanov@gmail.com); Tel.: +7-950-051-3095 (F.L.)

**Abstract:** The term deviation frequency denotes the boundary between the variable part of the amplitude and phase scintillation spectrum and the part of uninformative noises. We suggested the concept of the “characteristic deviation frequency” during the observation period which is defined as the most probable value of the deviation frequency under current local conditions. This work is a case study of the characteristic deviation frequency ( $f_d$ ) registered for GPS, GLONASS, Galileo and SBAS signals under quiet and weakly disturbed geomagnetic conditions in April 2021 at the mid-latitude GNSS station. Our results demonstrated that the  $f_d$  value for all signal components of GPS, GLONASS and GALILEO signals varied within 15-22 Hz. The characteristic deviation frequency was 20 Hz for the mentioned GNSS signals. In difference, the deviation frequency was limited within 13-20 Hz for SBAS with the lower characteristic deviation frequency at 18 Hz. We assume that the concept of the characteristic deviation frequency can be used to determine the optimal sampling rate of the GNSS carrier phase data for the ionospheric studies. The characteristic deviation frequency can also characterize the state of the regular trans-ionospheric radio channel.

**Keywords:** ionosphere; scintillations; carrier phase; GNSS; GPS; GLONASS; Galileo; SBAS; GNSS signals; deviation frequency

## 1. Introduction

Global Navigation Satellite Systems (GNSS) form part of a technological basis for different applications [1]. Their data is widely used for fundamental research tasks in different fields, for example in geodynamics [2], radio propagation environment including the GNSS remote sensing (GNSS-RO) [3] and GNSS Reflectometry of Earth surface (GNSS-R) [4]. In particular, one of the important geophysical studies that was carried out on the basis of GNSS signal processing was the study of the Earth's ionosphere and upper atmosphere [5- 7].

In many cases the main measured parameter of satellite vehicle (SV) signals is the carrier phase that is characterized by the lowest multipath noise level and the highest measurement accuracy. Various stochastic techniques report normally distributed carrier phase noise of 2 mm and code range noise of 0.5-0.8 m [8]. Such precise measurements allow us to detect the effects of rather weak geophysical events and eventually reconstruct the structure of the ionosphere.

Determination of optimum sensitivity of the carrier phase lock loop (PLL) is an important task for the remote sensing of the ionosphere. The PLL sensitivity depends on both the internal noises and the sampling rate of carrier phase measurements [9]. The selected measurement sensitivity can be considered optimal if, at a given noise level of measurements and at a given sampling rate, the

probability of weak event detection at the background of the uninformative noise within the phase variation spectrum is the highest.

Besides, the lower boundary in the spectrum of the phase variations (at which weak disturbances can still be registered) may be considered as the boundary of regular ionosphere. Further, we call it the boundary of the non-variability of the ionosphere. Studies that are focused on estimation of this boundary and its dependence on observation conditions are of particular importance for geophysical research advances.

McCaffrey and Jayachandran [10] suggested the “deviation frequency” term to denote the boundary between the variable part of the amplitude and phase scintillation spectrum and the part of uninformative noise in the spectrum. Developing this idea, we suggest introducing the concept of the characteristic deviation frequency during the observation period which is defined as the most probable value of the deviation frequency under current local conditions. We assume that the characteristic deviation frequency is both an estimate of the optimal sensitivity of the PLL and the boundary of non-variability of the ionosphere under the current conditions.

The aim of this work is to estimate the characteristic deviation frequency under particular observation conditions. The research tasks are to reveal the features of variations of the characteristic deviation frequency for GPS, GLONASS, GALILEO and SBAS satellites, types of satellite signals, time of day and the level of geomagnetic activity.

## 2. Data and processing method

The measurements of GNSS signal carrier phase were performed during April 13-16, 2021 with use of the multi-system multi-band navigation receiver Javad Delta-G3T connected to the RingAnt-G3T antenna [11]. The equipment was installed at the ISTP station (geographic coordinates 52.24°N, 104.26°E; geomagnetic coordinates 42.70°N, 177.43°E). The station belongs to the SibNet GNSS receiver network [12]. Figure 1 shows variations of Kp and SYM-H geomagnetic indices during the considered period.

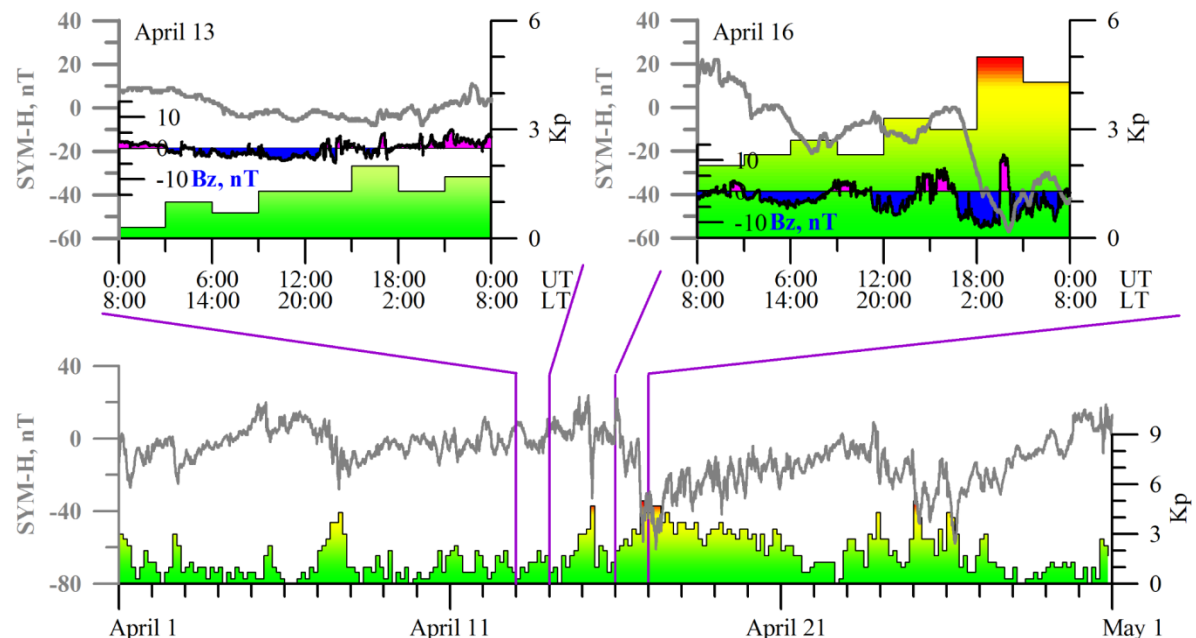


**Figure 1.** Variations of SYM-H and Kp indices and Bz-component of the interplanetary magnetic field during April 13<sup>th</sup> (upper left panel) and April 16<sup>th</sup>, 2021 (upper right panel). The Southward Bz-component is marked with the blue color and northward with light purple. General picture of SYM-H and Kp variations during April 1-30, 2021 (lower panel).

The intensity of the geomagnetic storm on April 16, 2021 was weak. SYM-H index did not demonstrate the Storm sudden commencement features. The SYM-H was not decreasing below -21 nT during the first part of the day, then it decreased sharply after 16:35 UT achieving the lowest

value of -57 nT at 20:02 UT. The Kp index reached the value equal to 5 during the period of 18:00-21:00 UT.

Thus, the main phase of the storm occurred in the local midnight sector. This means the minimal background electron concentration level. Such conditions imply the appearance of weak ionospheric disturbances registered at the border of the stationary of the ionosphere. Therefore, we chose the period of this storm for our analysis.

The level of carrier phase measurement noises significantly differs for signals of different systems and for different signal components [13-15]. This issue is important for estimation of the characteristic deviation frequency in the spectrum of phase variations and scintillations. Hence, the carrier phase noise for the signal components at L1, L2 and L5 frequencies of GPS, GLONASS, GALILEO and SBAS satellites were studied first (Table 1). The measurements were performed with a 50 Hz sampling rate. The signal components description mentioned in Table 1 can be found in the data format description available at [16].

**Table 1.** Considered GNSS signal components.

Navigation system	Signal components				
GPS	L1C	L1W	L2W	L2X	L5X
GLONASS	L1C	L1P		L2C	L2P
GALILEO		L1X			L5X
SBAS		L1C			L5I

We applied the following procedure for deviation frequency estimation. (1) Abnormal data and phase cycle slips were excluded. (2) Phase ambiguity was resolved by means of polynomial filtering. (3) Phase de-trending with use of 5 min moving average window was applied. The window width was chosen based on the results of [9] according to which phase fluctuations caused by small-scale irregularities should have the period of several seconds or less. Indeed, Pi et al. [7] reported a period of ~ (2-13) s and Forte and Radicella [17] reported ~ (0.4-5) s.

After preprocessing, a fast Fourier transform was applied to the phase data series. We did not apply Hanning window as in work [10], because of uncertainty of filter parameter choice under the unknown spread and behavior of deviation frequencies. The deviation frequency was determined at the logarithmic spectrum of phase variations as a “break point” at which the maximum decrease in the slope of the spectrum passes into near-zero decrease in a given frequency range. When performing this analysis, the frequency range from 5 to 25 Hz in the spectrum was studied, in which the deviation frequency was expected to vary.

At the first stage, the level of phase measurement noise for signals of different navigation systems, different frequencies and components were analyzed. The second-order derivative of the signal carrier phase was used as the noise magnitude (Please, see the methodology description in [14]). Table 2 provides RMS estimates for the noise of phase measurements for signals from different systems and components.

**Table 2.** RMS of the measurement noises of GNSS signal phase.

Navigation system	Signal component / RMS of the noise (2 $\pi$ cycle)				
GPS	L1C	L1W	L2W	L2X	L5X
	0.017	0.017	0.010	0.014	0.007
GLONASS	L1C	L1P	L2C	L2P	-
	0.014	0.015	0.013	0.014	
GALILEO	L1X		-		L5X
	0.019				0.006
SBAS	L1C		-		L5I
	0.035				0.027

According to Table 2, the level of the carrier phase noise for the similar types of components and signal frequencies of GPS, GLONASS and Galileo does not differ much. At the same time, RMS of the phase measurements for SBAS signals is 1.5-3 times higher, which is in accordance with the known results by [18]. The lowest noise level among the considered signal frequencies and components was detected for L5 frequency.

### 3. Discussion of results

#### 3.1. Deviation frequency estimates for different GNSS signal components

Figure 2 shows the histograms of distribution of the deviation frequency ( $f_d$ ) for signal components L1X and L5X of GALILEO satellites during 24 hours.

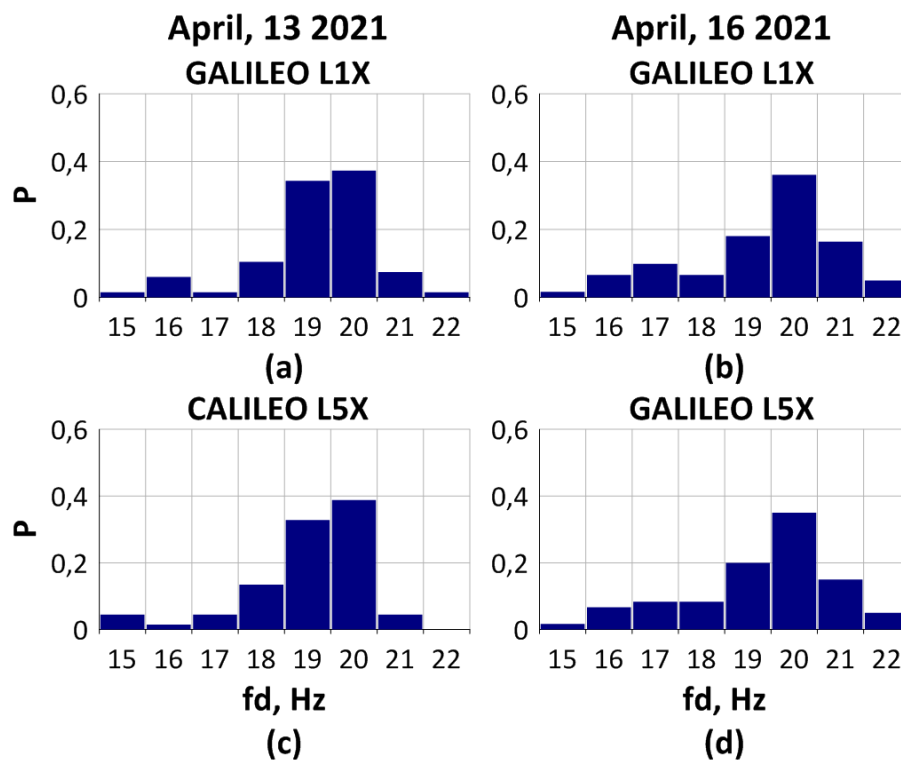


**Figure 2.** Deviation frequency distribution on April 13, 2021 (a,c) and April 16, 2021 (b,d) for GALILEO signals.

The deviation frequency value varied within 15-22 Hz during both days. The most probable deviation frequency in either day of two and for all signal components was 20 Hz. The character of distribution shown for L1X and L5X components under the same conditions has no fundamental difference. At the same time, the carrier phase noise level for the L5X component is significantly lower than for the L1X component (Table 2). Moreover, the histograms constructed for the control day of April 13<sup>th</sup> and the geomagnetically disturbed day of April 16<sup>th</sup> differ essentially. Histograms for the quiet day are characterized by more gradual rise at their left part. In contrast, the most probable deviation frequency is pronounced more clearly at the histograms for the disturbed day.

Figures 3 and 4 present the similar histograms for the signal components of GLONASS satellites and GPS satellites respectively.

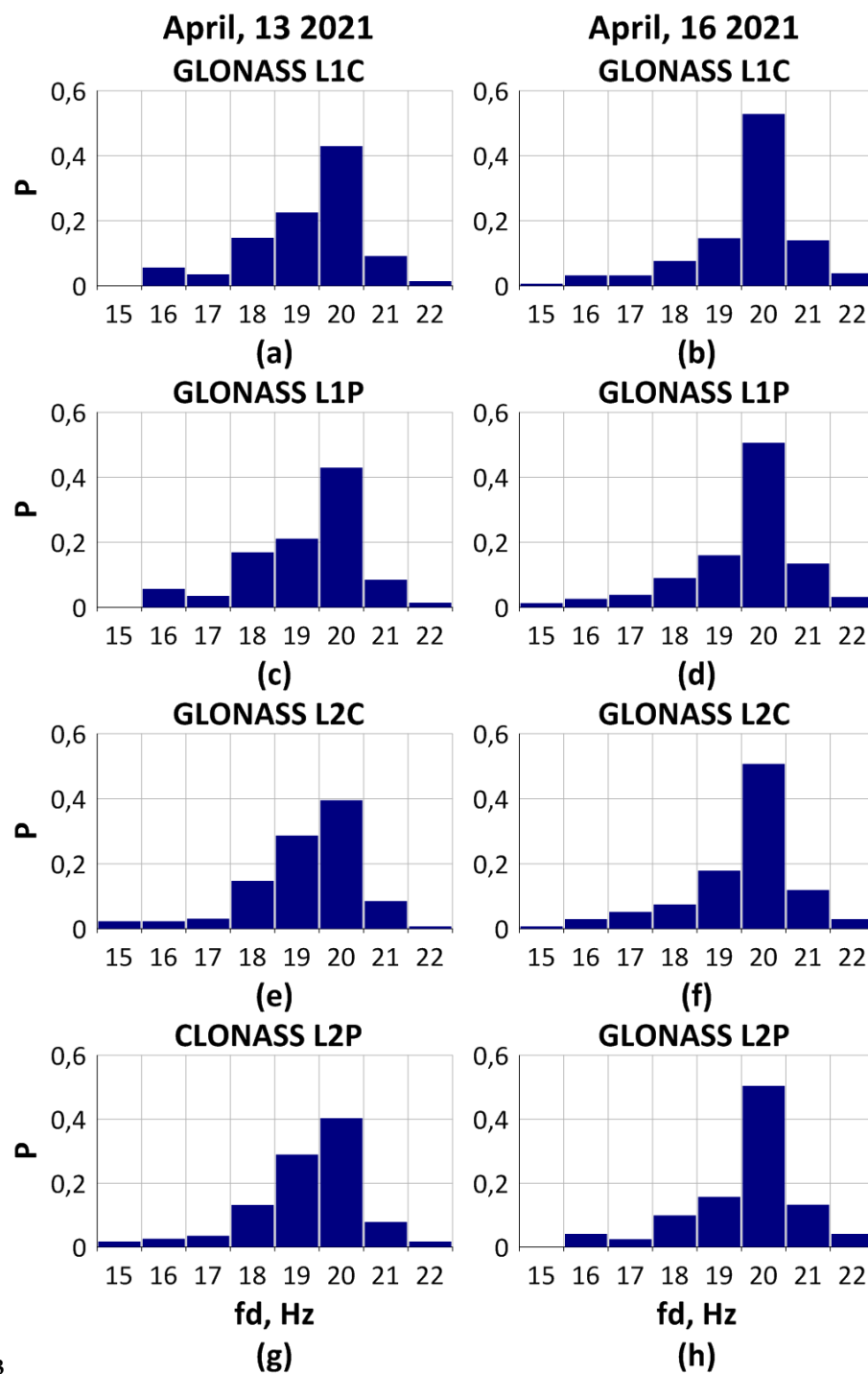
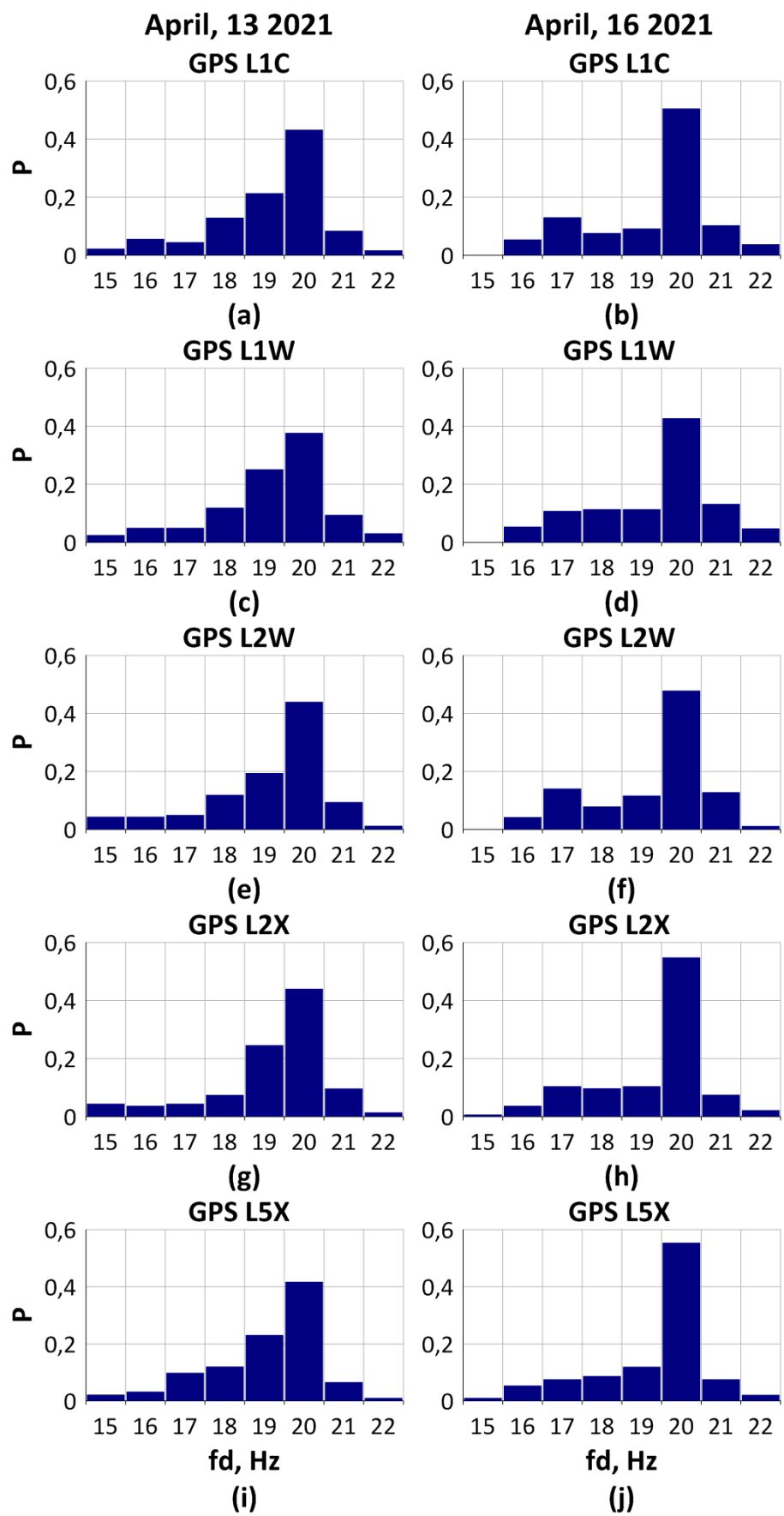


Figure 3. The same as in Figure 2 but for the signal components of GLONASS signals (Table 1).



**Figure 4.** The same as in Figure 2 but for the signal components of GPS signals (Table 1).

The character of distributions at histograms constructed for all GPS and GLONASS signal components under the same conditions has no fundamental difference as well. Deviation frequency again varies within 15-22 Hz. Though for some components this range is narrower – within 16-22 Hz (Figure 3a,c,h and Figure 4b,d,f). When comparing histograms in Figure 2 no significant difference of histogram form is shown. However, the characteristic deviation frequency of 20 Hz in Figures 3 and 4 has higher probability under geomagnetically disturbed conditions (0.43-0.55 for GPS, GLONASS and ~0.35 for GALILEO satellites). It can be noted the smoother increase of deviation frequency at the lower frequencies area during the quiet day of April 13<sup>th</sup> (Figure 3a,c,e,g and Figure 4a,c,e,g,i). It is also worth noting the rather uniform appearance deviation frequency level in histograms for GPS with the only exception of the 20 Hz peak during geomagnetically disturbed day (Figure 4 right panels).

Figure 5 shows the distribution of deviation frequency of carrier phase for L1X and L5I components of SBAS satellite signals during 24 hours. The measurements were obtained for three SBAS satellites whose angular characteristics are given in Table 3.

**Table 3.** Characteristics of SBAS satellite observations.

SBAS Satellite Number	Mean Elevation, deg	Mean Azimuth, deg
S28	27.08	206.22
S32	29.39	193.58
S37	26.60	152.02

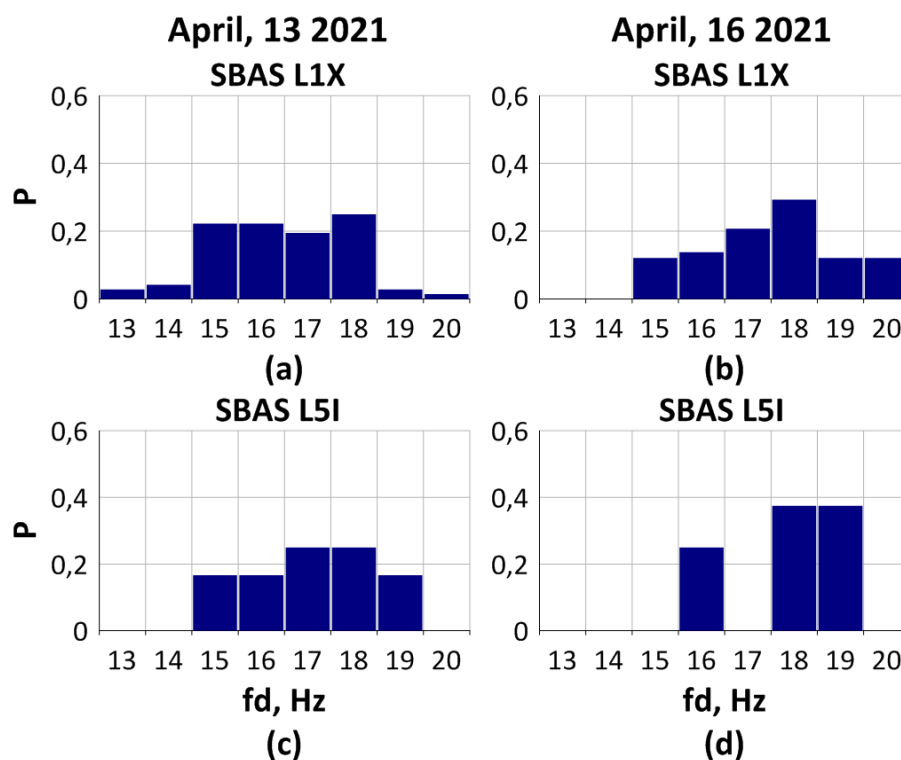


**Figure 5.** The same as in Figure 2 but for the L1X and L5I components of SBAS signals.

According to Table 3, all observed SBAS satellites were concentrated in one narrow southwest sector and at low elevation angles. Consequently, spatial variability of the ionosphere due to the line-of-site movement through different ionospheric/atmospheric regions may not be taken into account.

The histogram form in Figure 5 differs significantly from the histograms shown in Figures 2-4. The deviation frequency variations are limited within 13-20 Hz. Moreover, in general the deviation frequency value is lower. The most probable frequency can be determined with confidence only in



one case of four in Figure 5 (in panel b). For example, the characteristic deviation frequency in panel a of Figure 5 is 18 Hz with probability of 0.25, and it is 15 or 16 Hz with the probability of 0.22 for each of them. In contrast, in case of panel b of the same figure the characteristic deviation frequency is pronounced much clearer at 18 Hz. Other two histograms in Figure 5 show no clear maximum. Nevertheless, on the quiet day of April 13th lower values were seen at lower frequencies. In general, under disturbed conditions the maximum is observed more clearly and can be noted within 18-19 Hz (Figure 5b,d).

### 3.2. Deviation frequency dependence on geomagnetic conditions

The results discussed in the previous section showed rather high stability of characteristic deviation frequency at 20 Hz under particular conditions. This allows us to suggest that this characteristic frequency is primarily associated with the boundary of the regular ionosphere under current conditions. To test this assumption the analysis of variations of the most probable deviation frequency value was performed. Here, the characteristic deviation frequency was estimated for each hour separately but based on all the signal components of all systems with only SBAS excluded.

Figure 6 (upper panels) shows the deviation frequency variations during 24 hours. The local noon and the night period are indicated by the red arrow and blue rectangle respectively. The lower panels of the figure present the variation of the characteristic deviation frequency 20 Hz during 24 hours. The results for the quiet day are shown in the left panels and for the disturbed day in the right panels.

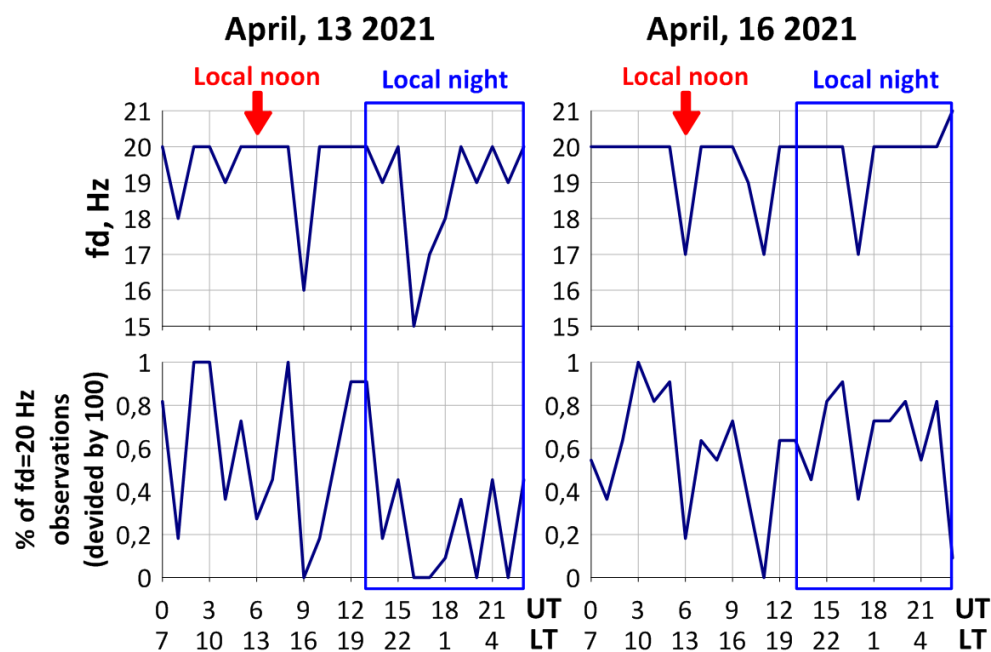


**Figure 6.** The deviation frequency variations (**upper panels**) and variations of the characteristic deviation frequency 20 Hz (**lower panels**) on April 13<sup>th</sup> (**left**) and April 16<sup>th</sup> (**right**).

Figure 6 (upper panels) proves that the deviation frequency at 20 Hz is characteristic during the most part of the day on April 16<sup>th</sup> (under weak geomagnetic disturbance). At the same time, there are short periods of the frequency drastically decreasing to ~17 Hz. The first and the third decreases occurred near the time of local noon and local midnight. This is different for the quiet day on April 13<sup>th</sup> when the deviation frequency varied more significantly (up to 15 Hz) and more frequently. The most profound through of deviation frequency values (15 Hz) corresponded to the local midnight as in the previous case.

Figure 6 (lower panels) shows that the characteristic deviation frequency 20 Hz is highly variable during 24 hours. For both days, no particular tendency can be revealed for the character of these variations. Nevertheless, the probability of observation of the characteristic deviation



frequency 20 Hz at some particular time moments was higher under quiet conditions on April 13<sup>th</sup> (up to 0.9-1.0) than under disturbed conditions (up to 0.8).

#### 4. Conclusions

The concept of the characteristic deviation frequency can be used to determine the optimal sampling rate of the GNSS carrier phase data for the ionosphere studies. In this work the characteristic deviation frequency is considered optimal if its further increase does not provide more information on the small-scale structure of the ionosphere. The characteristic deviation frequency can also characterize the state of the regular transionospheric radio channel.

According to our results, in general the characteristic deviation frequency is rather stable during the short time intervals of observations (1 hour). However, its value can vary significantly during 24 hours (within 15-21 Hz). This is in accordance with the current knowledge on the physical ionospheric structure [19-23].

The maximal probability of the characteristic deviation frequency 20 Hz did not exceed 0.8 under geomagnetically disturbed conditions and reached the values of 0.9-1.0 under quiet conditions. The increase of this probability can indicate the increase of the spatial-temporal stability of the ionosphere under quiet conditions. Correspondently, its decrease implies the presence of the disturbance effects that change the phase spectrum slope.

The probability distribution of the characteristic deviation frequency obtained from SBAS data differs from the probability distribution of the other GNSS signals significantly. We showed that the carrier phase noise for SBAS signals is notably higher than for the signals of other GNSS. This is in accordance with the results of [18]. Probably, the plasmasphere could impact the characteristic deviation frequency for SBAS signals. This hypothesis should be tested with further experiments and analysis of data. Moreover, the signals of geostationary SBAS satellites passed from the same narrow angular sector. It means that spatial variability of the ionosphere due to the line-of-site movement through different ionospheric/atmospheric regions did not impact on the deviation frequency variations significantly. This circumstance is absent for the radio propagation of signals from medium-orbit (and lower orbital) GNSS constellations. The data of geostationary BeiDou satellites which is characterized by the same phase noise level as GPS/GLONASS may be used for checking this hypothesis further.

**Supplementary Materials:** SYM-H and Bz indices data were obtained from the NASA/GSFC's Space Physics Data Facility's OMNIWeb service (<https://omniweb.gsfc.nasa.gov>). Kp-index data were obtained from GFZ German Research Centre for Geosciences (<ftp://ftp.gfz-potsdam.de>) [24].

**Author Contributions:** V.D. developed the conceptualization of this work; V.D. and Y.Y. designed the experiments; E.D. and M.S. provided the data processing, and performed the simulations the experiments; all the authors participated in the analysis of the results; V.D. and M.S. prepared the manuscript with contributions from all the authors. All authors have read and agreed to the published version of the manuscript.

**Funding:** This work was performed under the Russian Science Foundation Grant No. 17-77-20005.

**Acknowledgments:** We thank Dr. Artem Vesnin for his help in GNSS data acquisition.

**Conflicts of Interest:** The authors declare no conflict of interest.

#### References

1. TS-02-20-382-EN-N. Power-efficient positioning for THE Internet of Things. White paper by European GNSS Agency. 2020, doi:10.2878/437669.
2. Asteriadis, G.; Schwan, H. GPS and terrestrial measurements for detecting crustal movements in a seismic area. *Surv. Rev.* **1998**, *34*, 447–454, doi.org/10.1179/sre.1998.34.269.447.
3. Jin, S.; Cardellach, E.; Xie, F. *GNSS Remote Sensing: Theory, Methods and Applications*; Springer: Dordrecht, The Netherlands, 2014.
4. Padokhin, A. M.; Kurbatov, G. A.; Nazarenko, M. O.; Smolov, V. E. GNSS Reflectometry of the Black Sea Level in the Experiments at the Stationary Oceanographic Platform. *Moscow University Physics Bulletin* **2018**, *73*(4), 422–427, doi:10.3103/S0027134918040112.

5. Afraimovich, E.L.; Astafyeva, E.I.; Demyanov, V.V.; Edemskiy, I.K.; Gavriluk, N.S.; Ishin, A.B.; Kosogorov, E.A.; Leonovich, L.A.; Lesyuta, O.S.; Perevalova, N.P.; et al. Review of GPS/GLONASS studies of the ionospheric response to natural and anthropogenic processes and phenomena. *J. Space Weather Space Clim.* **2013**, *3*, A27, doi:10.1051/swsc/2013049.
6. Hernández-Pajares, M.; Juan, J.M.; Sanz, J.; Orus, R.; Garcia-Rigo, A.; Feltens, J.; Komjathy, A.; Schaer, S.C.; Krankowski, A. The IGS VTEC maps: A reliable source of ionospheric information since 1998. *J. Geophys.* **2009**, *83*, 263–275, doi.org/10.1007/s00190-008-0266-1.
7. Pi, X.; Mannucci, A.J.; Lindqwister, U.J.; Ho, C.M. Monitoring of global ionospheric irregularities using the worldwide GPS network. *Geophys. Res. Lett.* **1997**, *24*, 2283–2286, doi.org/10.1029/97GL02273.
8. Kersten, T.; Paffenholz, J.-A. Feasibility of Consumer Grade GNSS Receivers for the Integration in Multi-Sensor-Systems. *Sensors* **2020**, *20*, 2463, doi.org/10.3390/s20092463.
9. Demyanov, V.V.; Yasyukevich, Y.V.; Jin, S.; Sergeeva, M.A. The Second-Order Derivative of GPS Carrier Phase as a Promising Means for Ionospheric Scintillation Research. *Pure Appl. Geophys.* **2019**, *176*, 4555–4573, doi:10.1007/s00024-019-02281-6.
10. McCaffrey, A.M.; Jayachandran, P.T. Spectral characteristics of auroral region scintillation using 100 Hz sampling. *GPS Solut* **2017**, *21*, 1883–1894, doi.org/10.1007/s10291-017-0664-z.
11. JAVAD GNSS Receiver External Interface Specification. Available online: [http://download.javad.com/manuals/GREIS/GREIS\\_Reference\\_Guide.pdf](http://download.javad.com/manuals/GREIS/GREIS_Reference_Guide.pdf). (accessed on October 1, 2021).
12. Yasyukevich, Y.V.; Perevalova, N.P.; Vesnin, A.M. SibNet—Siberian Global Navigation Satellite System Network: Current state. *Sol. Terr. Phys.* **2018**, *V. 4, N 4*, 63–72, doi:10.12737/stp-44201809.
13. Padma, B.; Kai, B. Performance analysis of dual-frequency receiver using combinations of GPS L1, L5, and L2 civil signals. *J. Geod.* **2019**, *93*, 437–447, doi:10.1007/s00190-018-1172-9.
14. Demyanov, V.; Sergeeva, M.; Fedorov, M.; Ishina, T.; Gatica-Acevedo, V.J.; Cabral-Cano, E. Comparison of TEC Calculations Based on Trimble, Javad, Leica, and Septentrio GNSS Receiver Data. *Remote Sens.* **2020**, *12*, 3268, doi.org/10.3390/rs12193268.
15. Prochniewicz, D.; Grzymala, M. Analysis of the Impact of Multipath on Galileo System Measurements. *Remote Sens.* **2021**, *13*, 2295, doi.org/10.3390/rs13122295.
16. IGS Analysis Center Coordinator (ACC). Available online: <http://acc.igs.org/misc/rinex304.pdf>. (accessed on October 5, 2021).
17. Forte, B.; Radicella, S. M. Problems in data treatment for ionospheric scintillation measurements. *Radio Science* **2002**, *37(6)*, 8-1–8-5, doi:10.1029/2001rs002508.
18. Kunitsyn, V.E.; Padokhin, A.M.; Kurbatov, G.A.; Yasyukevich, Y.V.; Morozov, Y.V. Ionospheric TEC estimation with the signals of various geostationary navigational satellites. *GPS Solut.* **2016**, *20*, 877–884, doi.org/10.1007/s10291-015-0500-2.
19. Aarons J. The role of the ring current in the generation or inhibition of equatorial F layer irregularities during magnetic storms. *Radio Science* **1991**, *26(4)*, 1131-1149, doi: 10.1029/91RS00473.
20. Muella, Marcio T. A. H.; Duarte-Silva, Marcelo H.; Moraes, Alison O.; de Paula, Eurico R.; de Rezende, Luiz F. C.; Alfonsi, Lucilla; Affonso, Bruno J. Climatology and modeling of ionospheric scintillations and irregularity zonal drifts at the equatorial anomaly crest region. *Ann. Geophys.* **2017**, *35*, 1201–1218, doi.org/10.5194/angeo-35-1201-2017.
21. Mendillo, M. Storms in the ionosphere: Patterns and processes for total electron content. *Rev. Geophys.* **2006**, *44*, RG4001, doi:10.1029/2005RG000193.
22. Immel, T. J.; Mannucci, A. J. Ionospheric redistribution during geomagnetic storms. *J. Geophys. Res. Space Physics* **2013**, *118*, 7928–7939, doi:10.1002/2013JA018919.
23. Ratovsky, K.G.; Klimenko, M.V.; Klimenko, V.V.; Chirik, N.V.; Korenkova, N.A.; Kotova, D.S.. After-effects of geomagnetic storms: statistical analysis and theoretical explanation. *Solar-Terrestrial Physics* **2018**, *Vol. 4. Iss. 4*, P. 26–32. DOI: 10.12737/stp-44201804.
24. Matzka, J.; Bronkalla, O.; Tornow, K.; Elger, K.; Stolle, C., Geomagnetic Kp index. V. 1.0. GFZ Data Services, 2021, <https://doi.org/10.5880/Kp.0001>.